Electronic Supplementary Material (ESI) for Dalton Transactions.

Tri- and hexanuclear Ni^{II}–Mn^{II} complexes of a N_2O_2 donor unsymmetrical ligand: Synthesis, structures, magnetic properties and catalytic oxidase activities

Prithwish Mahapatra[a], Michael G. B. Drew[b], Ashutosh Ghosh*[,a]

[a]*Department of Chemistry, University College of Science, University of Calcutta, 92, A. P. C. Road, Kolkata 700009, India, E-mail: ghosh_59@yahoo.com*

[b]*School of Chemistry, The University of Reading, P.O. Box 224, Whiteknights, Reading RG6 6AD, UK.*

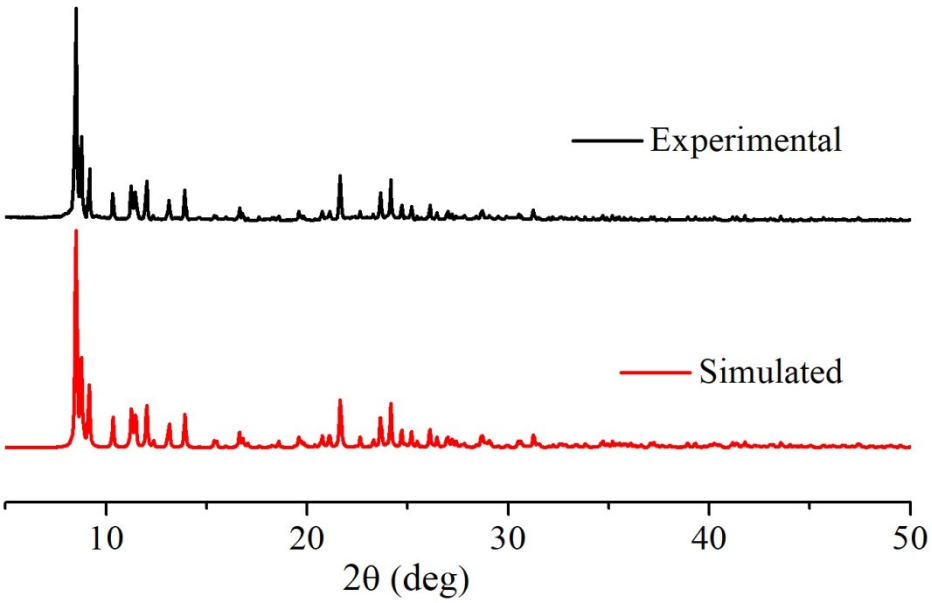

Figure S1. X-Ray powder diffractogram of complex **2**.

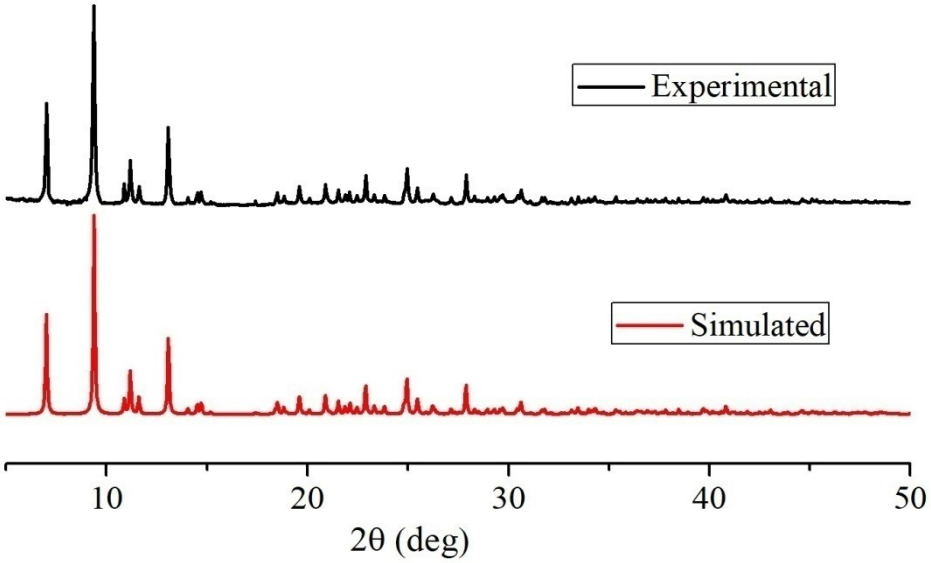

Figure S2. X-Ray powder diffractogram of complex **3**.

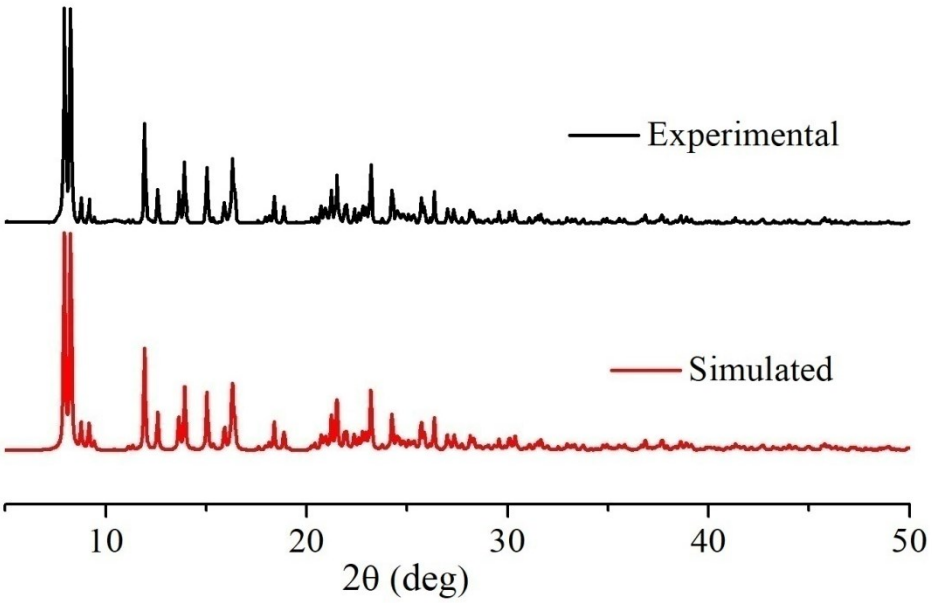

Figure S3. X-Ray powder diffractogram of complex **4**.

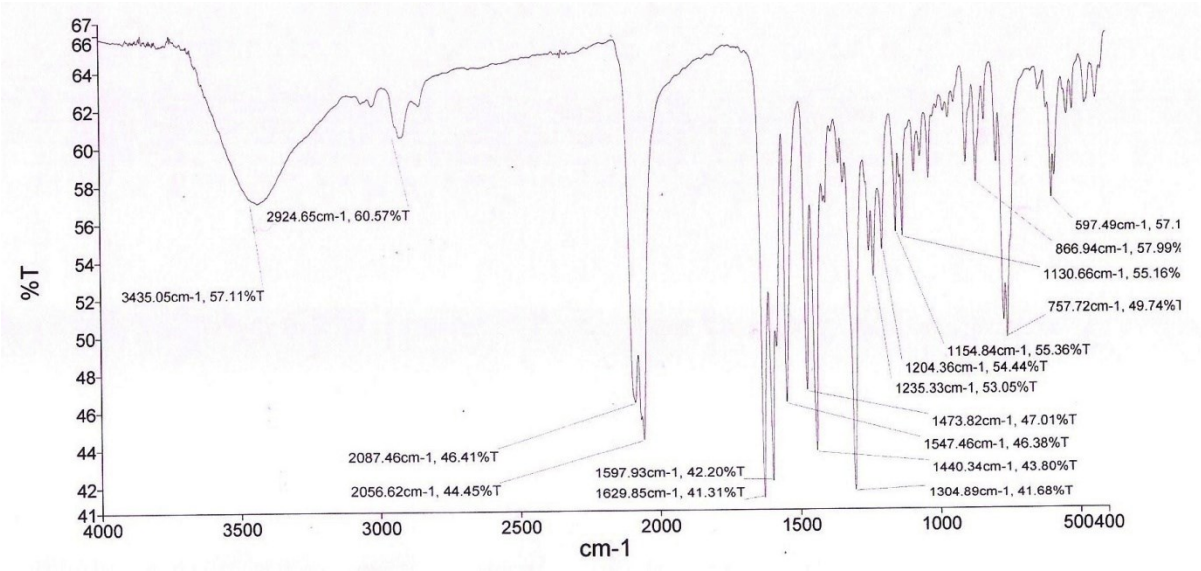

Figure S4. Representative IR spectrum of complex **2**.

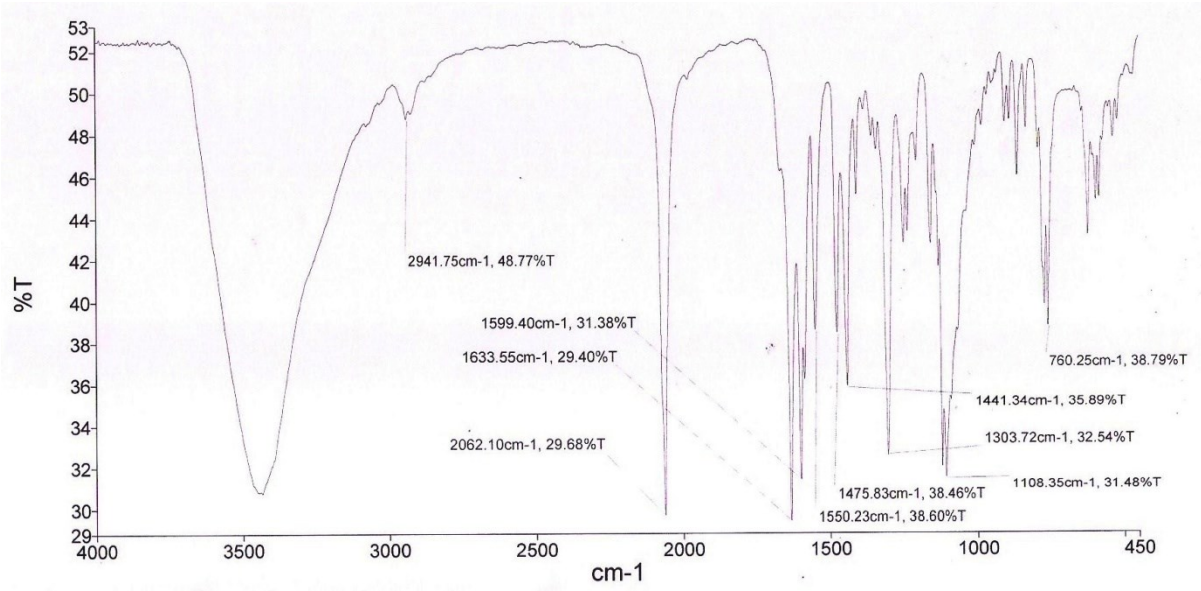

Figure S5. Representative IR spectrum of complex **3**.

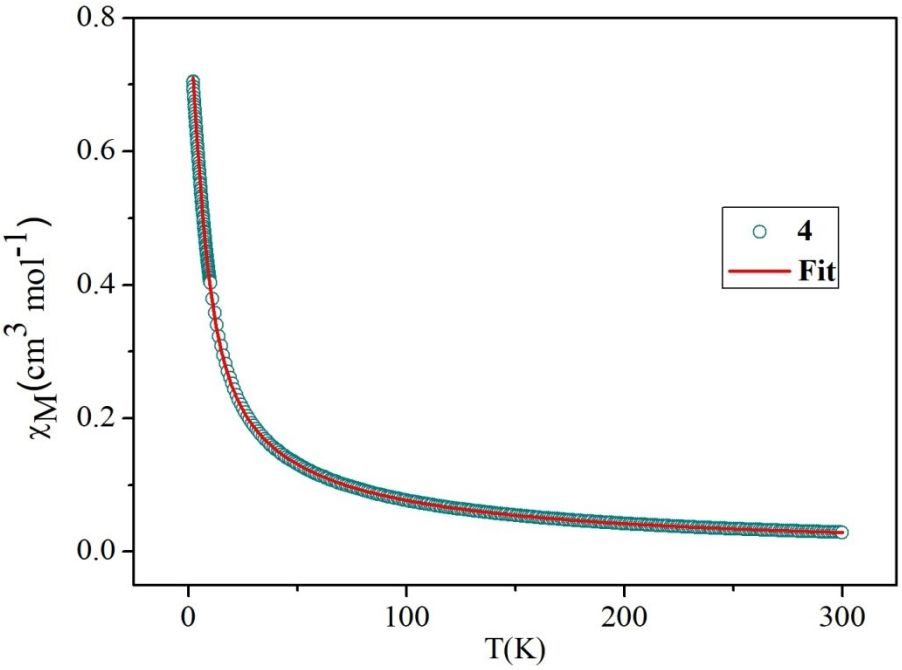

Figure S6. Thermal variations of the χ_M for complex **4**.

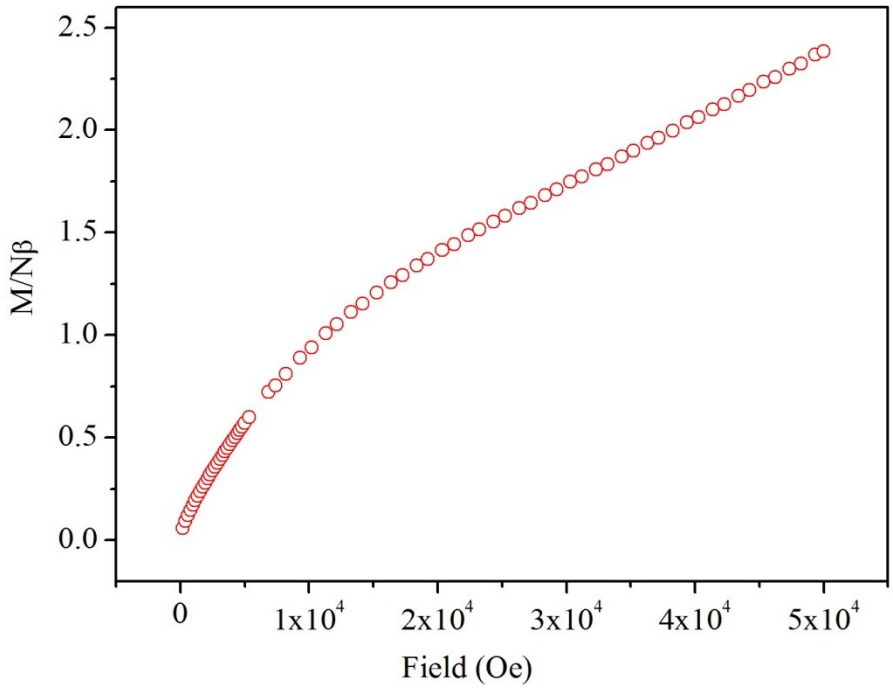

Figure S7. Isothermal magnetizations at 2 K for complex **4**.

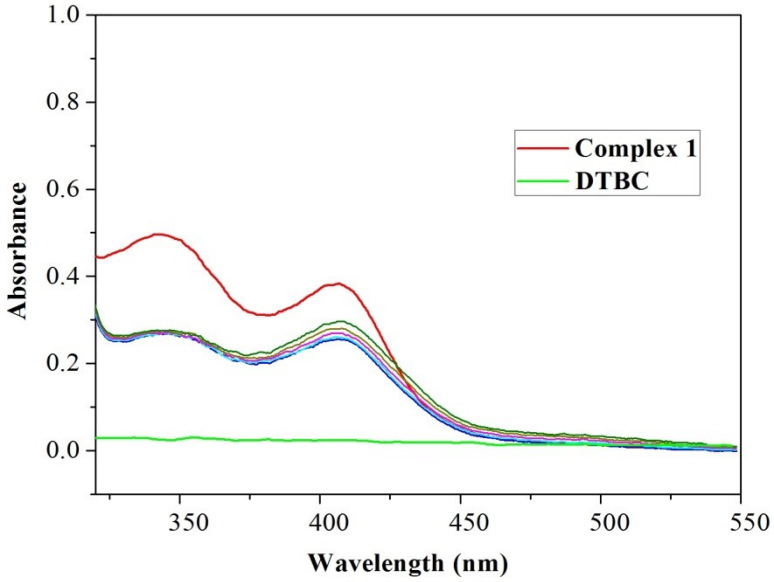

Figure S8. Increase in the 3,5-DTBQ band at around 400 nm after the addition of 3,5-DTBC (1×10^{-2} M) to the methanolic solution of complex **1**.

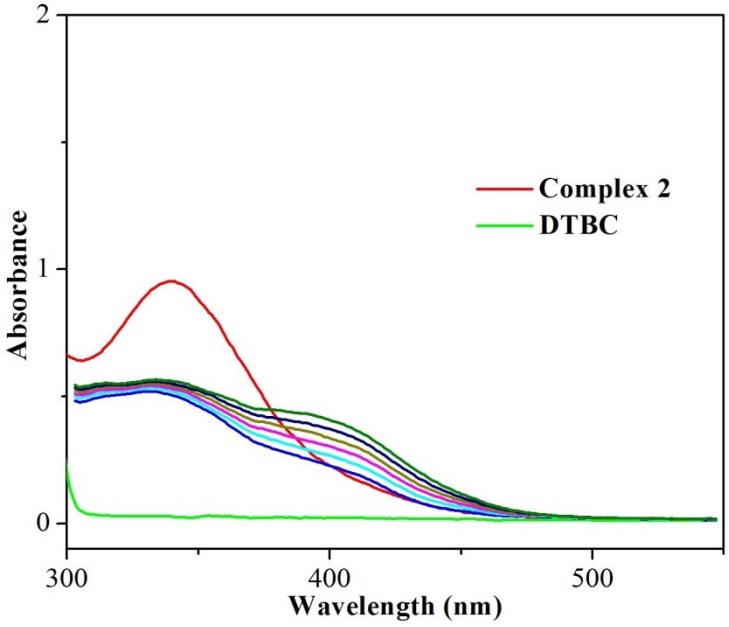

Figure S9. Increase in the 3,5-DTBQ band at around 400 nm after the addition of 3,5-DTBC (1×10^{-2} M) to the methanolic solution of complex **2**.

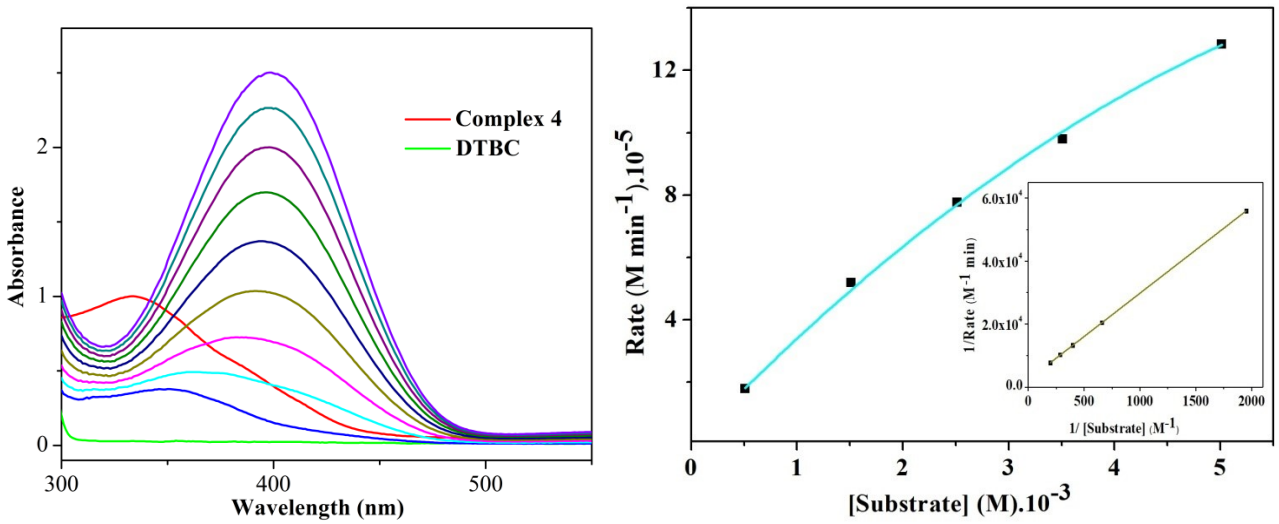

Figure S10. Increase in the 3,5-DTBQ band at around 400 nm after the addition of 3,5-DTBC (1×10^{-2} M) to the methanolic solution of complex **4** (5×10^{-5} M) (left) and plot of the rate *vs*. substrate concentration (right). Inset shows the corresponding Lineweaver–Burk plot of **4**. The UV-spectra were recorded at 5 minute intervals.

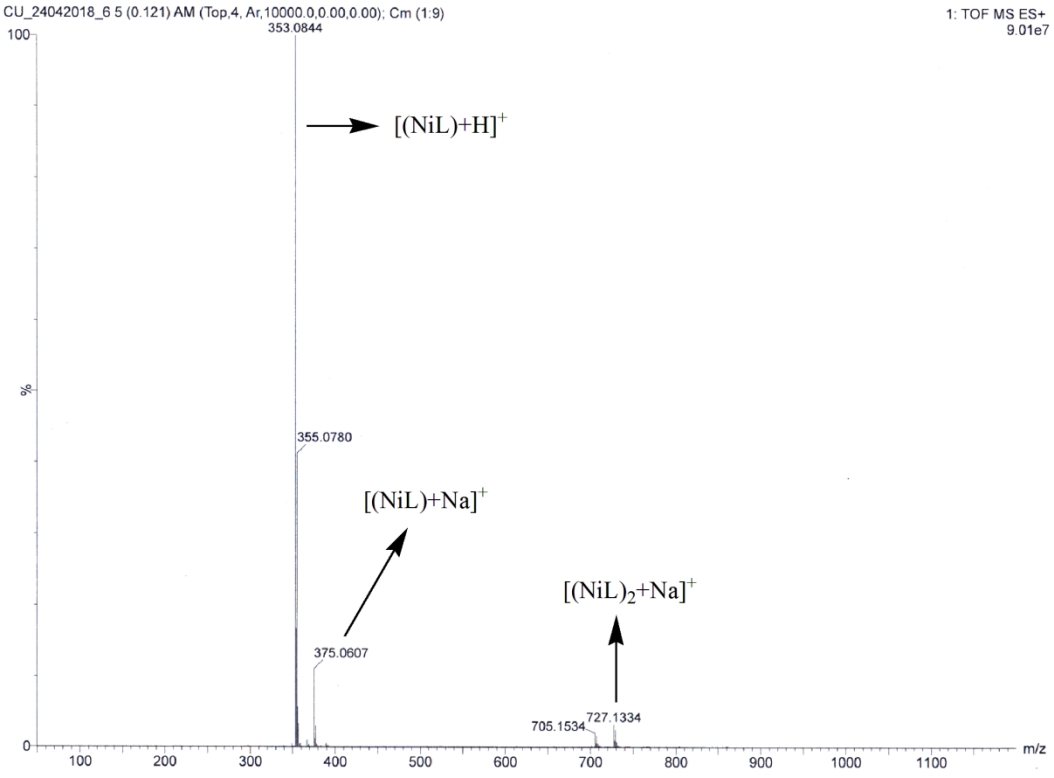

Figure S11. Representative ESI mass spectrum of complex **2**.

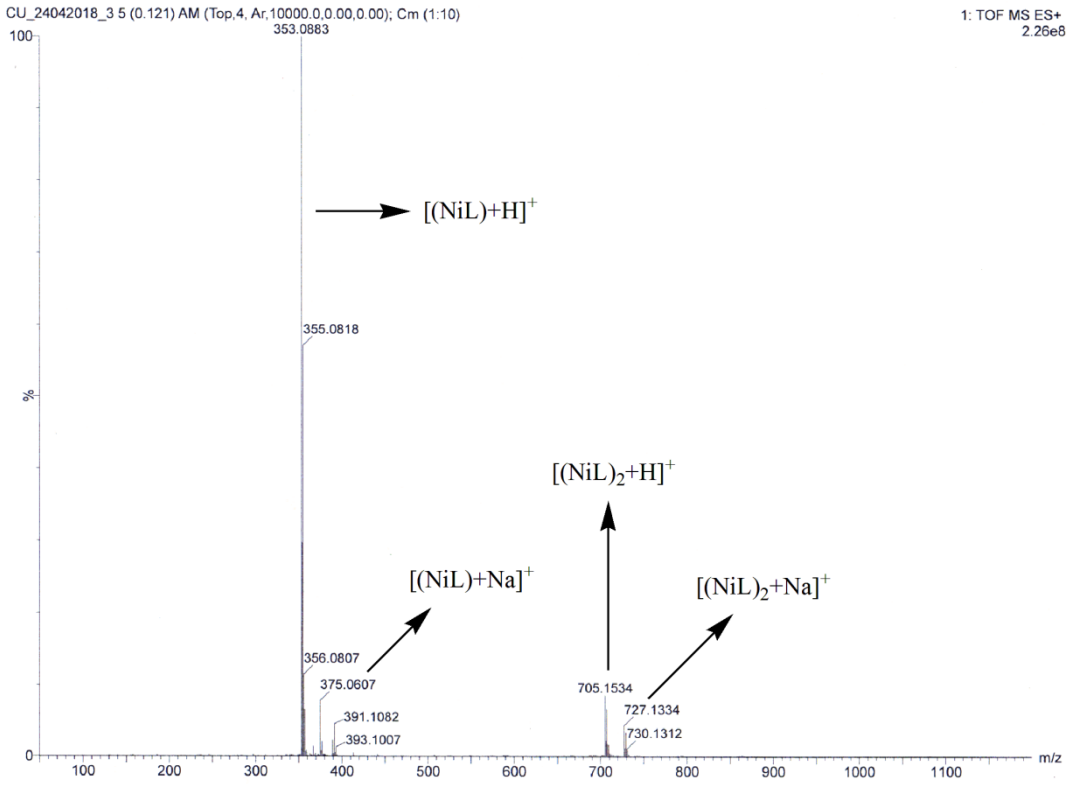

Figure S12. Representative ESI mass spectrum of complex **3**.

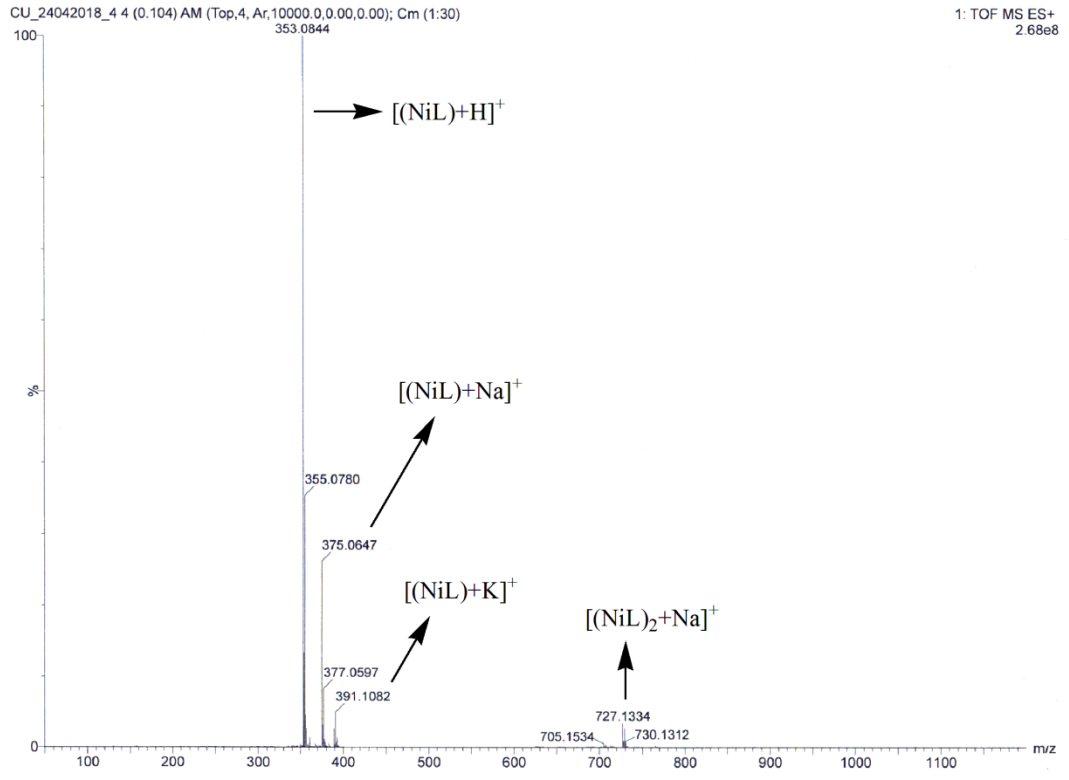

Figure S13. Representative ESI mass spectrum of complex **2** with DTBC.

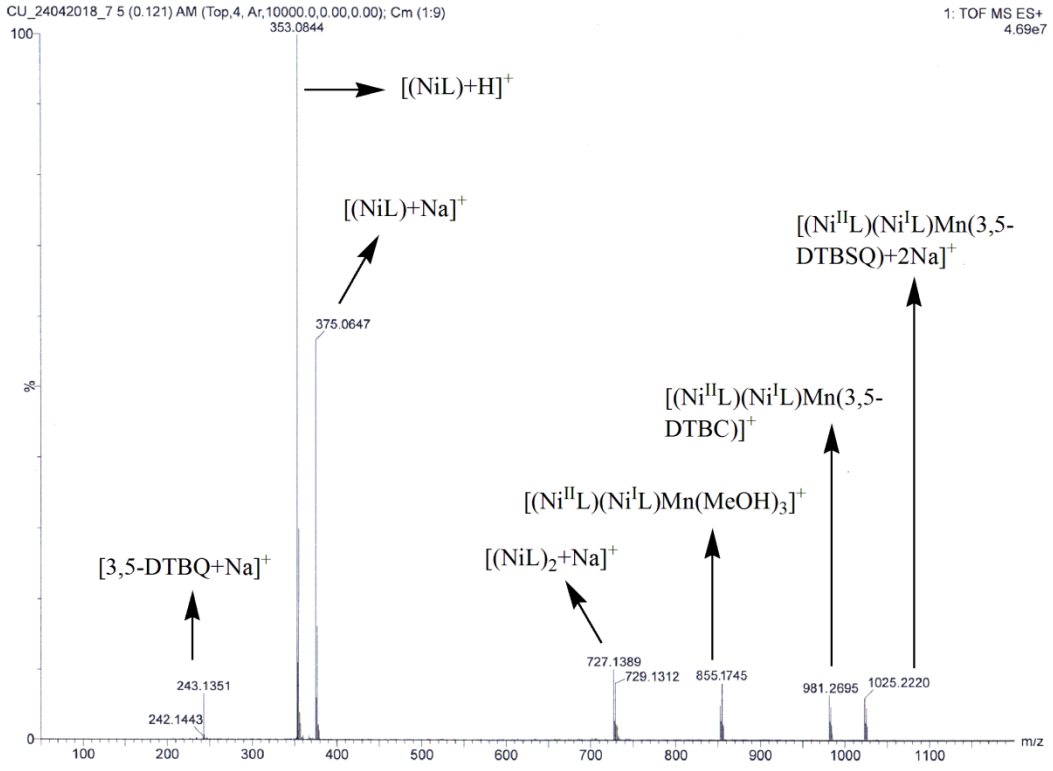

Figure S14. Representative ESI mass spectrum ofcomplex **3** with DTBC.

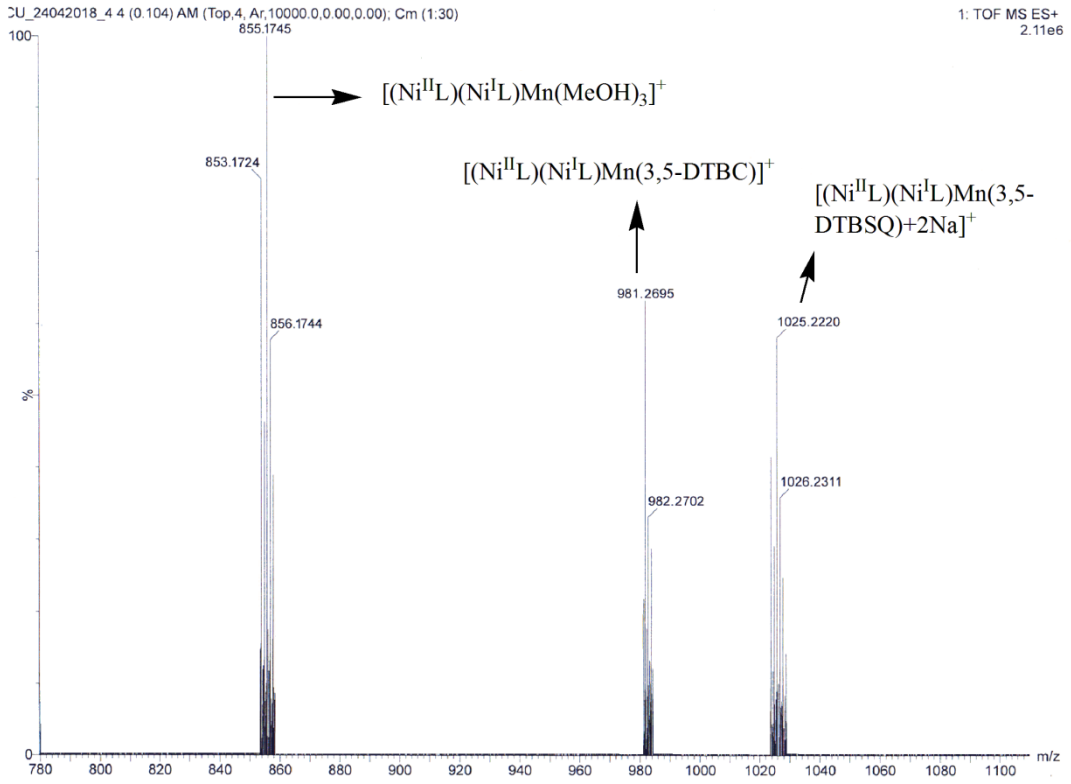

Figure S15. Representative ESI mass spectrum of complex **3** with DTBC.

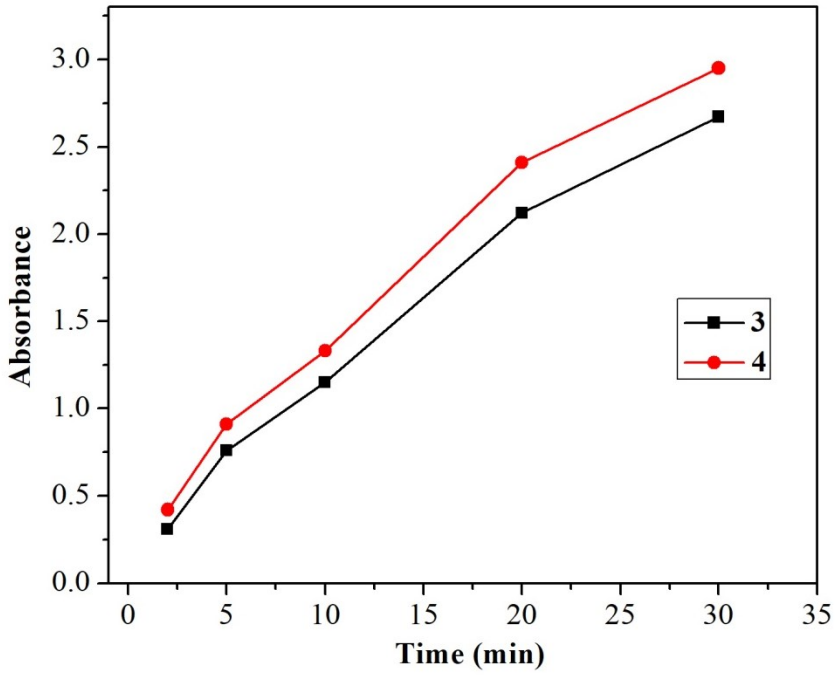

Figure S16. Plot of H_2O_2 estimation of complexes **3**–**4**.

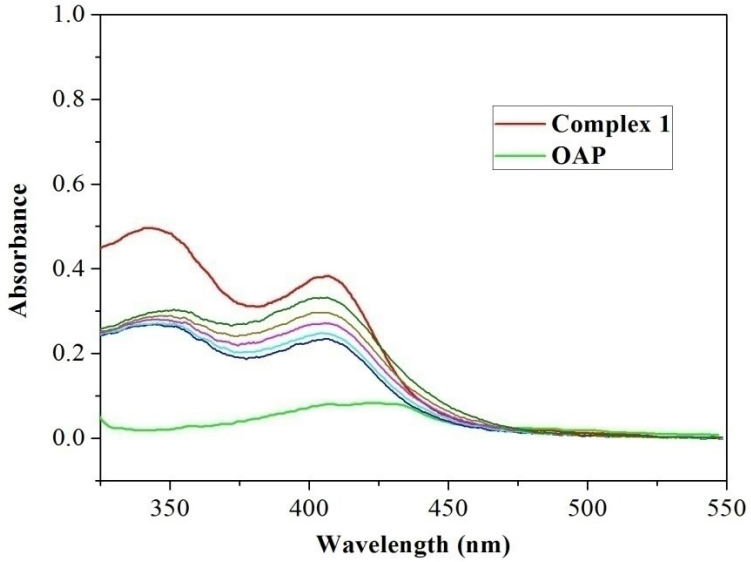

Figure S17. Increase in the APX band at around 425 nm after the addition of OAP (1×10^{-2} M) to the methanolic solution of complex **1**.

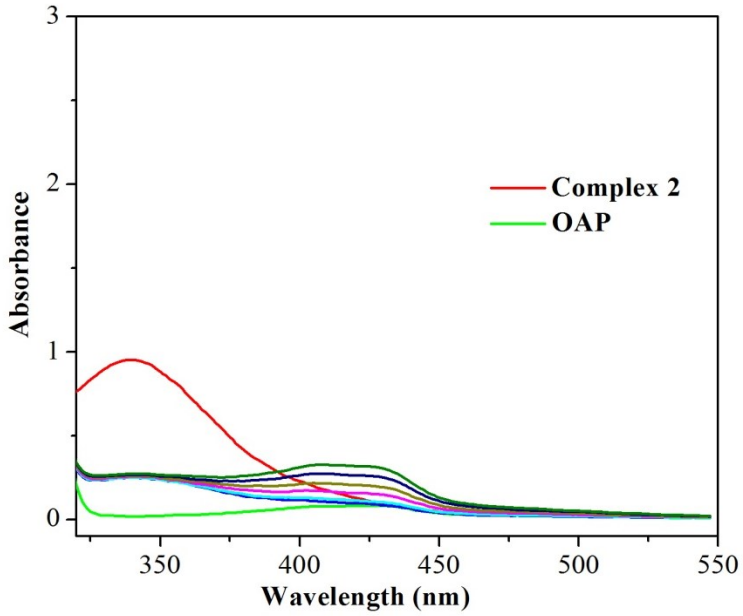

Figure S18. Increase in the APX band at around 425 nm after the addition of OAP (1×10^{-2} M) to the methanolic solution of complex **2**.

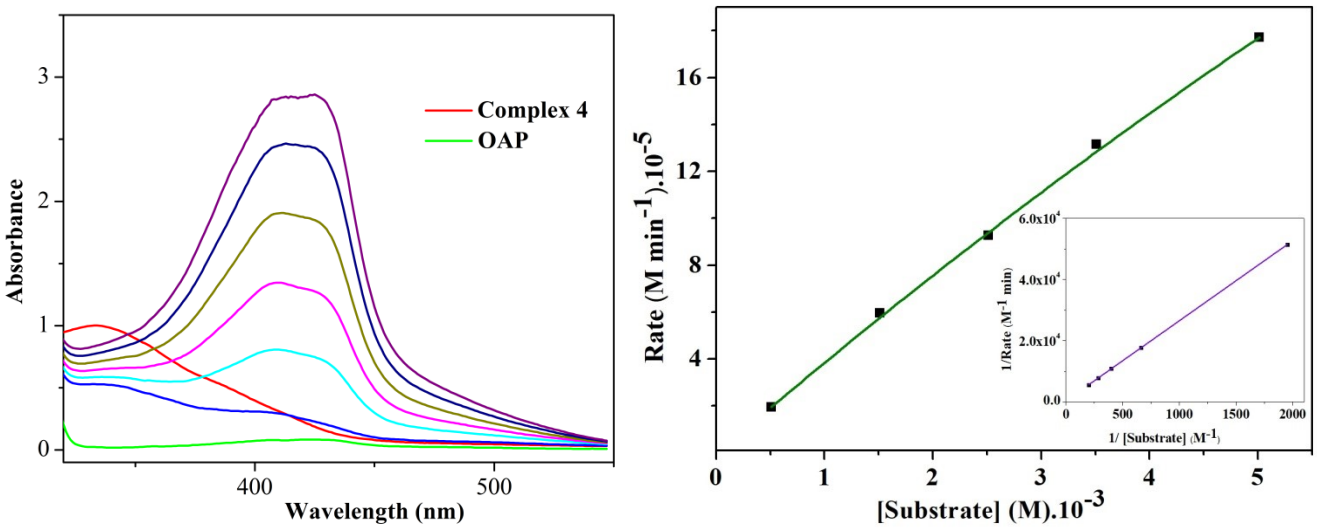

Figure S19. Increase in the aminophenoxazinone band at around 425 nm after the addition of *o*-aminophenol (1×10^{-2} M) to the methanolic solution of complex **4** (5×10^{-5} M)(left) and plot of the rate *vs*. substrate concentration (right). Inset shows the corresponding Lineweaver–Burk plot of **3**. The UV-spectra were recorded at 5 minute intervals.

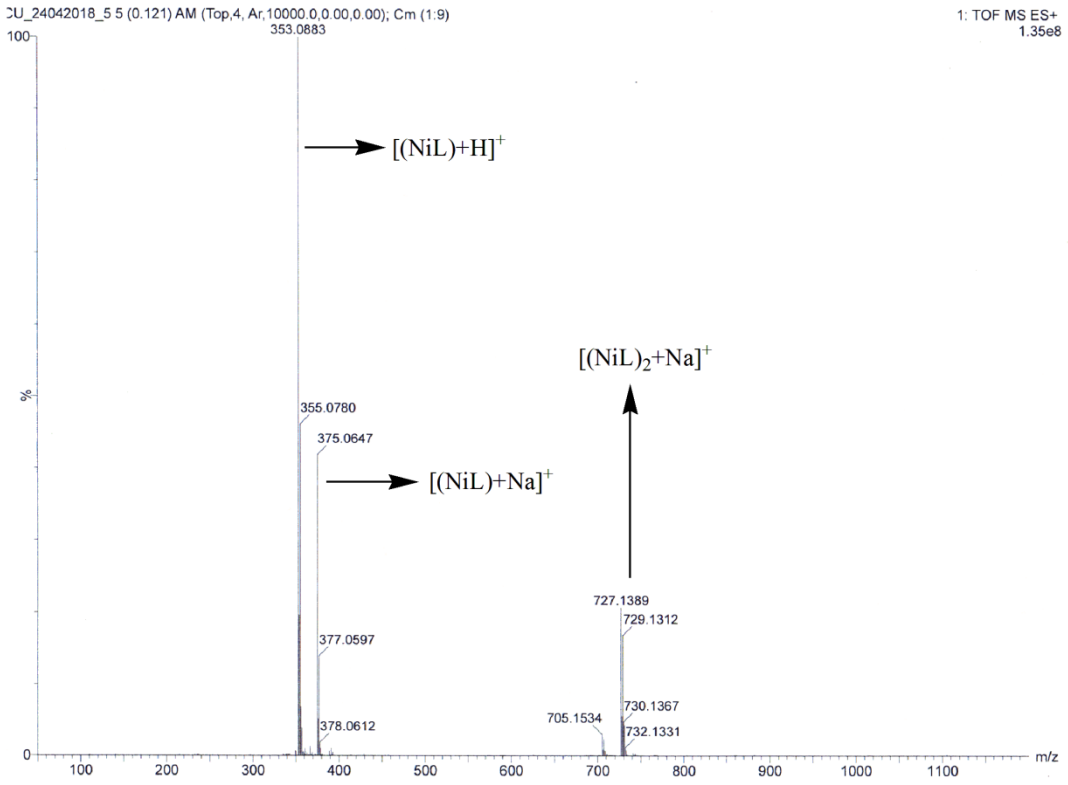

Figure S20. Representative ESI mass spectrum of complex **2** with OAP.

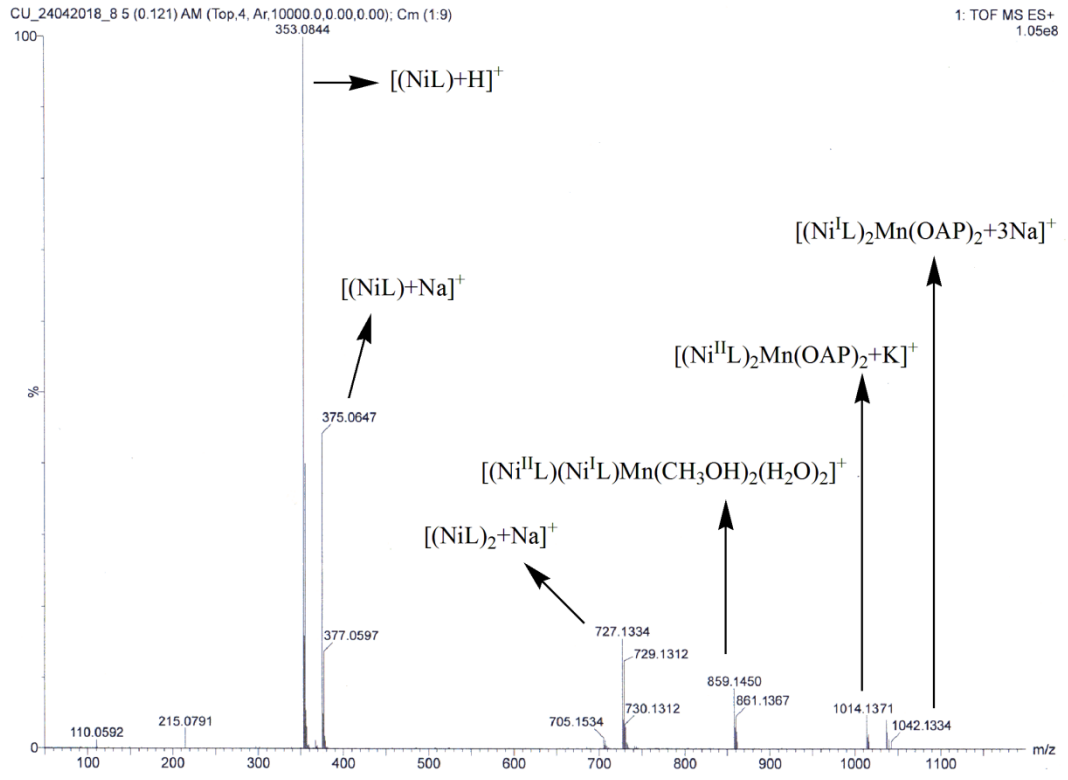

Figure S21. Representative ESI mass spectrum of complex **3** with OAP.

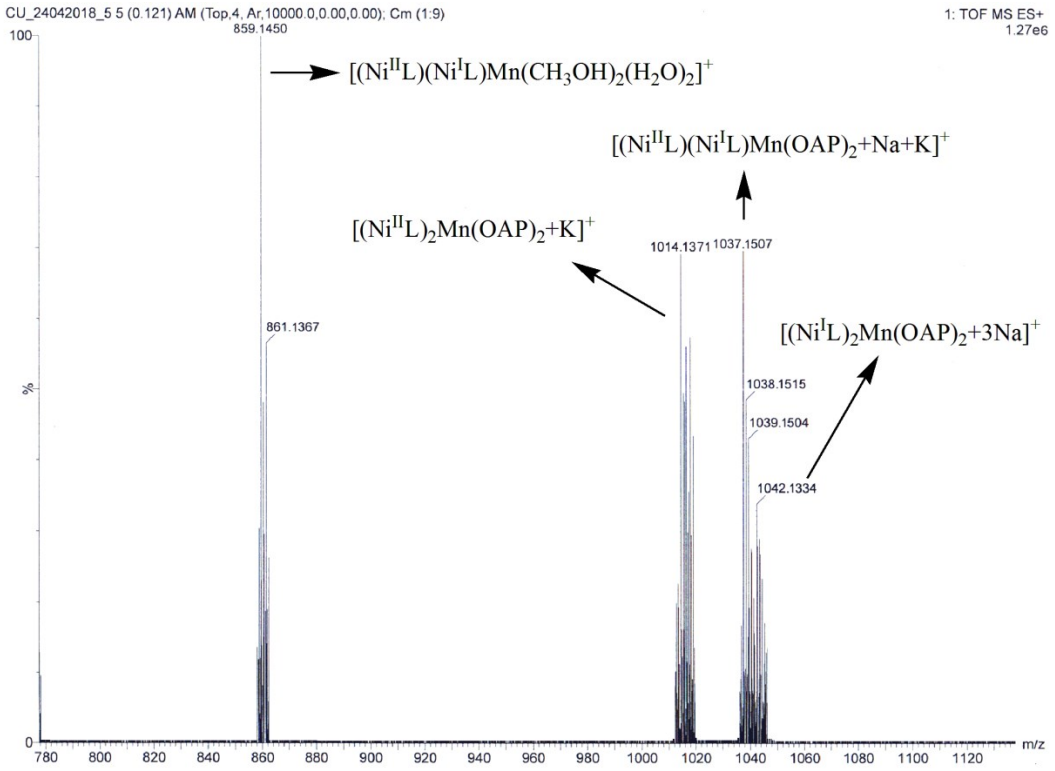

Figure S22. Representative ESI mass spectrum of complex **3** with OAP.

Table S1. Bond distances (Å) and angles (°) for complex **1**.

Compound	**1**
Ni(1)-O(11)	1.873(2)
Ni(1)-O(31)	1.888(2)
Ni(1)-N(23)	1.920(2)
Ni(1)-N(19)	1.970(2)
O(11)-Ni(1)-O(31)	83.30(8)
O(11)-Ni(1)-N(23)	172.83(10)
O(11)-Ni(1)-N(19)	89.68(9)
O(31)-Ni(1)-N(23)	91.78(9)
O(31)-Ni(1)-N(19)	172.54(9)
N(19)-Ni(1)-N(23)	95.44(9)

Table S2. Bond distances (Å) and angles (°) for complexes **2**–**4**.

Compound	**2**	**3**	**4**
	X=N(2)	X=O(1W)	X=O(1W)
Ni(1)-O(11)	1.901(5)	1.926(3)	1.864(3)
Ni(1)-O(31)	1.930(5)	1.919(4)	1.839(3)
Ni(1)-N(23)	1.933(7)	1.931(4)	1.871(4)
Ni(1)-N(19)	1.965(6)	1.979(5)	1.899(4)
Ni(2)-O(41)	1.915(6)	1.915(3)	1.840(4)
Ni(2)-O(61)	1.901(6)	1.927(4)	1.870(4)
Ni(2)-N(53)	1.925(10)	1.926(5)	1.869(5)
Ni(2)-N(49)	1.961(10)	1.984(5)	1.903(6)
Mn(3)-O(31)	2.383(5)	2.243(3)	2.250(3)
Mn(3)-O(11)	2.111(5)	2.133(4)	2.118(3)
Mn(3)-X	2.121(7)	2.187(4)	2.165(5)
Mn(3)-N(1)	2.133(8)	2.156(4)	2.134(5)
Mn(3)-O(61)	2.269(6)	2.371(3)	2.263(4)
Mn(3)-O(41)	2.112(5)	2.134(4)	2.105(4)
O(11)-Ni(1)-O(31)	82.6(2)	81.63(15)	81.58(14)
O(11)-Ni(1)-N(23)	167.6(3)	174.47(18)	174.49(16)
O(11)-Ni(1)-N(19)	91.2(2)	89.00(16)	89.23(16)
O(31)-Ni(1)-N(23)	93.0(2)	92.90(17)	94.05(17)
O(31)-Ni(1)-N(19)	162.9(3)	170.01(16)	169.69(16)
N(19)-Ni(1)-N(23)	96.0(3)	96.51(18)	95.39(18)
O(41)-Ni(2)-O(61)	81.7(2)	82.03(16)	82.02(16)
O(41)-Ni(2)-N(53)	174.7(4)	171.33(18)	171.9(2)
O(41)-Ni(2)-N(49)	87.5(3)	89.87(18)	89.3(2)
O(61)-Ni(2)-N(53)	93.2(4)	92.83(17)	94.8(2)
O(61)-Ni(2)-N(49)	168.9(3)	166.95(16)	166.67(19)
N(49)-Ni(2)-N(53)	97.5(4)	96.4(2)	95.1(3)
O(31)-Mn(3)-O(41)	82.7(2).	86.31(13)	86.33(13)

O(31)-Mn(3)-X	163.5(2)	163.66(16)	163.79(19)
O(41)-Mn(3)-X	108.7(2)	104.20(16)	108.3(2)
O(31)-Mn(3)-N(1)	90.5(2)	95.76(16)	98.09(18)
O(41)-Mn(3)-N(1)	98.3(3)	101.54(16)	94.2(2)
X-Mn(3)-N(1)	99.4(3)	94.35(18)	88,0(2)
O(31)-Mn(3)-O(61)	76.7(2)	78.12(12)	85.97(13)
O(41)-Mn(3)-O(61)	69.3(2)	67.83(13)	67.63(14)
X-Mn(3)-O(61)	95.8(2)	94.09(15)	93.1(2)
N(1)-Mn(3)-O(61)	162.9(2)	167.83(17)	161.2(2)
O(31)-Mn(3)-O(11)	68.2(2)	70.04(13)	67.18(12)
O(41)-Mn(3)-O(11)	145.0(2)	144.45(12)	146.51(14)
X-Mn(3)-O(11)	96.8(2)	94.74(15)	96.55(19)
N(1)-Mn(3)-O(11)	100.8(2)	106.77(16)	108.95(19)
O(61)-Mn(3)-O(11)	85.0(2)	81.23(13)	89.55(13)

Table S3. Catalytic activities of complexes **3**–**4** on 3,5-DTBC.

Complex	**Conc.**	**K_{cat}**	**V_{max}**	**Std. error**	**K_M**	**Std. error**
3	5×10^{-5}	984	4.10×10^{-4}	1.36×10^{-4}	3.31×10^{-2}	1.87×10^{-4}
4	2.5×10^{-5}	2081	4.34×10^{-4}	1.58×10^{-4}	3.15×10^{-2}	2.26×10^{-4}

Table S4. Quantitative estimation of H_2O_2 formation (%) with Time (min) during the catecholase reaction.

Complex	**Time (min)**	**2**	**5**	**10**	**20**	**30**
3	% of H_2O_2	10.12	26.45	37.24	71.41	84.52
4	% of H_2O_2	11.61	29.53	41.62	78.76	92.41

Table S5. Catalytic activities of complexes **3**–**4** on OAP.

Complex	Conc.	K_{cat}	V_{max}	Std. error	K_M	Std. error
3	5×10^{-5}	6351	2.65×10^{-3}	6.27×10^{-4}	1.38×10^{-2}	1.63×10^{-4}
4	2.5×10^{-5}	10545	2.20×10^{-3}	5.42×10^{-4}	1.54×10^{-2}	1.82×10^{-4}